Topologically Protected Generation of Stable Wall Loops in Nematic Liquid Crystals

Tomohiro Ouchi (大内智弘),[1] Koki Imamura (今村弘毅),[1] Kanta Sunami (角南寛太),[1]
Hiroyuki Yoshida (吉田浩之),[1,2,*] and Masanori Ozaki (尾﨑雅則)[1]
[1]*Division of Electrical, Electronic and Information Engineering, Graduate School of Engineering, Osaka University, 2-1 Yamada-oka, Suita, Osaka 565-0871, Japan*
[2]*Precursory Research for Embryonic Science and Technology (PRESTO), Japan Science and Technology Agency (JST), 4-1-8 Honcho, Kawaguchi, Saitama 332-0012, Japan*

(Received 29 December 2018; published 29 August 2019)

The nematic liquid crystal (LC) director field can contain defects that are both singular and nonsingular, but nonsingular defects with an integer winding number of the director are typically metastable because of their high energy. We demonstrate topology-mediated generation and stabilization of nonsingular wall loops in a sandwich-type LC cell by combining a patterned substrate with a planar substrate. We implement a design which imposes a topological constraint on a singular disclination loop such that it irreversibly annihilates upon application of a field, and it results in the generation of a stable nonsingular wall loop when the field is removed. Theoretical modeling agrees with experimental observations, providing insight into the wall generation mechanism and its stability. The concept to stabilize high-energy structures through orientation-patterning-defined topological constraints extends our ability to control orientationally ordered matter.

DOI: 10.1103/PhysRevLett.123.097801

The nematic liquid crystal (LC) is a phase in which the constituent rodlike molecules spontaneously orient along a single direction, referred to as the director. The nematic director field can accommodate defects that are either singular or nonsingular, characterized by the number of rotations of the director around the defect core [1,2]. Singular defects can exist as lines or points, and they have been studied from various perspectives, from testing topological theorems [3,4] to utilizing them to modulate the local physical properties [5] or as templates for dopant materials [6–12].

In comparison to singular defects, nonsingular defects are much less explored. Nonsingular defects occur as spatially localized excitations in the director field and have continuous structures that are topologically equivalent with a uniformly aligned nematic [2]. In a sandwich-type nematic cell with planar boundary conditions, nonsingular defects appear at the boundary of two topologically equivalent regions in the form of walls, with the director locally orienting perpendicular to the substrates [13–17]. However, the steep variation in the orientation makes them high energy such that wall loops formed at the isotropic-nematic phase transition shrink and disappear over time [13]. Also, the property of LCs to minimize their free energy creates a tendency for walls to split into lower energy disclinations (singular line defects) [6]. Consequently, the study of walls had been mainly limited to those that appear only under an external field [18], offering little freedom in their control. While the growing interest in defects has led to various strategies for the control of disclinations, such as the inclusion of colloidal particles [3,4,19] and use of patterned substrates [6,20–22], little attention has been paid on actively controlling nonsingular defects.

In this Letter, we present a strategy to stabilize arbitrarily shaped wall loops in an achiral nematic LC through the surface anchoring design of a sandwich-type cell. A combination of a uniform planar and a suitably patterned substrate generates a looped disclination, which, upon application and cessation of an electric field, is converted into a stable wall loop. The conversion makes use of the local incompatibility in director topology so that regeneration of the singular disclination is suppressed although it has lower energy than the wall. The wall position is well reproduced by theoretical modeling, clarifying the underlying stabilization mechanism. Our approach enables selective stabilization of high-energy defect structures, extending our control over orientationally ordered matter.

Figure 1 depicts the easy axis distributions to stabilize a circular wall loop. The easy axis on one substrate (the "patterned substrate") is patterned such that the azimuthal angle, $\varphi_p(r,\theta) = \varphi_{p(r)}$, is given by Eq. (1) in cylindrical coordinates, where the origin is placed at the pattern center:

$$\varphi_p(r) = -\frac{\pi}{r_0} r + \frac{3\pi}{2}, \qquad 0 \le r \le \frac{3r_0}{2}. \tag{1}$$

The azimuthal angle changes by π over a distance of r_0 and extends to $3r_0/2$. Another substrate (the "uniform substrate") is prepared to possess uniform orientation, and a

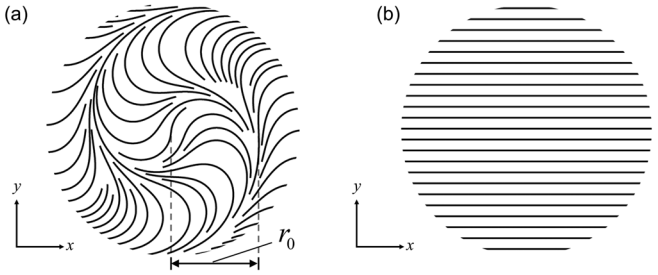

FIG. 1. Streamline representations of the orientational easy axis on the (a) patterned and (b) uniform substrates.

sandwich cell is fabricated using the two substrates so that the easy axis of the uniform substrate is parallel to the region of 0 radian on the patterned substrate.

A ∼8-μm-thick sandwich cell was prepared using two substrates coated with polyimide (JSR, AL1254) and photoalignment agent (DIC, LIA-03). The substrate with polyimide was rubbed unidirectionally, whereas the substrate with the photoalignment layer was patterned to possess the easy axis distribution of Fig. 1(a) using maskless photoalignment [22]. The photoalignment setup imprinted the local orientational easy axis over an area of 1024×768 pixels, where each pixel size was $\sim 1.3 \times 1.3\ \mu\text{m}^2$. The pattern was digitized to 3° steps and imprinted with a light dosage of 0.3 μJ/pixel. After cell fabrication, a nematic LC (5CB, Merck) was injected into the cell in the isotropic phase, and observed at 30 °C using a polarized optical microscope [polarized optical microscopy (POM), Nikon, LV100 POL].

Figure 2(a) shows a schematic of the LC-filled cell. A nematic LC confined between two substrates with different easy axis directions twists in the bulk to minimize the elastic free energy [1]. Because 5CB is achiral, the director twists in the direction that reduces the twist angle. The twist angle distribution expected from the pair of substrates used is shown in Fig. 2(c), where the twist angle is kept below $|\pi/2|$ in all regions. At $r = r_0$, the twist angle changes discontinuously by π and changes the twist direction from left ($r < r_0$) to right ($r > r_0$). The π jump in twist angle is accompanied by a singular disclination and appears as a black line floating in the LC.

Figures 2(d)–2(f) show POM images of the sample with $r_0 = 107\ \mu$m. Between crossed polarizers, light is transmitted where its polarization changes due to director twisting. The disclination loop appears as a thin dark line at approximately $r = r_0$, and it is also observed without the analyzer. Insertion of a first order retardation plate ($\lambda = 530$ nm) shows that the twist sense is inverted at the defect, but there is no tilt induced in the director since no significant change in birefringence occurs near the disclination.

Generally, disclinations possess a line tension and tend to shrink [1,23]. However, the easy axis on the patterned substrate is designed such that the elastic energy due to director distortion increases with disclination shrinkage. That is, because the twist angle can only change discontinuously at the disclination, its displacement from position r_0 to $(r_0 – \Delta r)$ causes the twist inversion to occur at twist angles of $(\pi\Delta r/r_0 \mp \pi/2)$ instead of $\mp\pi/2$. This increases the twist component of the elastic energy, which is proportional to the square of the twist rate [1]. The disclination loop is stabilized where the free energy of the disclination relieved by shrinkage is balanced by the increase in the elastic energy [22] [see also Sec. I of the Supplemental Material (SM) [24]].

After confirming the generation of a disclination loop, an electric field (1 kHz, 2.5 V) was applied between the substrates. The electric field reorients the director perpendicular to the substrates and untwists the director [1], causing the disclination to shrink and annihilate over time. When the field is removed after disclination annihilation, the disclination does not reappear, but a nonsingular wall loop is generated at $r \sim 1/2r_0$ [see Figs. 2(h)–2(j) and Movie 1 in the SM [24]]. The wall loop is stable and disappears only when the sample is heated into the isotropic phase, but upon reentering the nematic phase, the disclination reappears, implying that the configuration with the disclination has lower energy. The wall appears thicker than the disclination and can also be observed without the analyzer. Insertion of the retardation plate reveals a color change in regions separated by the wall, implying again a large change in twist angle at the wall. On the other hand, the color changes inside the wall, implying that now there is an out-of-plane tilt deformation of the director.

The above observations allow us to interpret the disclination-to-wall transition mechanism as follows. Consider a cross-section area of the cell containing a section of the disclination that runs perpendicular to the plane [Fig. 2(a)]. The topological properties of a line defect can be analyzed by taking a circular path around the disclination core and mapping the orientation along the path on a sphere representing all of the possible orientation directions (i.e., order parameter space) [2]. Defects in LCs are also commonly characterized by their strength: it is the number of 2π rotations of the director along a circular path that surrounds the defect, and it can take half integers or integers. In a three-dimensional nematic, defects with half-integer strength can be continuously transformed into a defect of strength $1/2$, and those with integer strength can be transformed into a uniformly aligned state with strength 0. Thus, the topological invariant, or charge, can take only two values, either $1/2$ or 0 (in terms of defect strength), and must be conserved according to the following: $1/2 + 0 = 1/2$ and $1/2 + 1/2 = 0$.

In Fig. 2(a), the disclination gives a contour on the order parameter space terminating at diametrically opposite points; it is a topologically stable singularity with charge $1/2$. Because there is another defect with opposite strength

on the other side of the loop (at $\theta = \pi$), shrinkage of the defect by the applied field causes the disclination to eventually annihilate and give a net defect strength of 0. When the field is removed, the most stable configuration would be to have the two disclinations repositioned at their initial positions (recall that this configuration is always obtained through a thermal phase transition). However, because the director is now everywhere continuous and free of singularities, there is locally a topological incompatibility that prohibits the regeneration of disclinations. Instead of returning to a state with two defects of charge $1/2$, the system is required to relax into a state with charge 0 everywhere, i.e., with 0 or integer defect strength.

Since shrinkage of the disclination loop causes the right-handed twist region (originally at $r > r_0$) to extend to below r_0, a configuration with strength 0 corresponds to one that is right-handed everywhere. On the other hand, the configuration with strength 1 corresponds to one that accommodates a wall with a 2π jump in twist angle [23,25]. A completely right-handed configuration would require the maximum twist angle to reach $3\pi/2$ at $r = 0$, whereas, although the wall has high energy density and its energy is proportional to its length, the maximum twist angle can be reduced to $\sim|\pi|$ if it is accommodated at $r = r_0/2$, where the easy axes on the substrates are parallel [Fig. 2(g)]. Thus, there is a competition between wall shrinkage and minimization of director twist acting in opposite directions, similar to the case of disclination. Stabilization of the wall occurs as a result of the LC relaxing into a topologically allowed configuration with lowest energy.

We analyze the free energy landscape of the director configuration with a wall loop and show that there is indeed an equilibrium loop radius that minimizes the energy. We base our analysis on a model for the wall proposed by Turner [15], which describes the director distribution using an analytical function with no singularities (Sec. II of the SM [24]). The Turner distribution has been found to be a close approximation to that obtained by minimizing the free energy numerically [17]. A cylindrical coordinate system is employed, with the uniform and patterned substrates placed at $z = -d/2$ and $d/2$, where d is the cell gap. A LC with splay, twist, and bend elastic constants of K_{11}, K_{22}, and K_{33} fills the cell and accommodates a circular wall loop with its center at the origin and radius r_w.

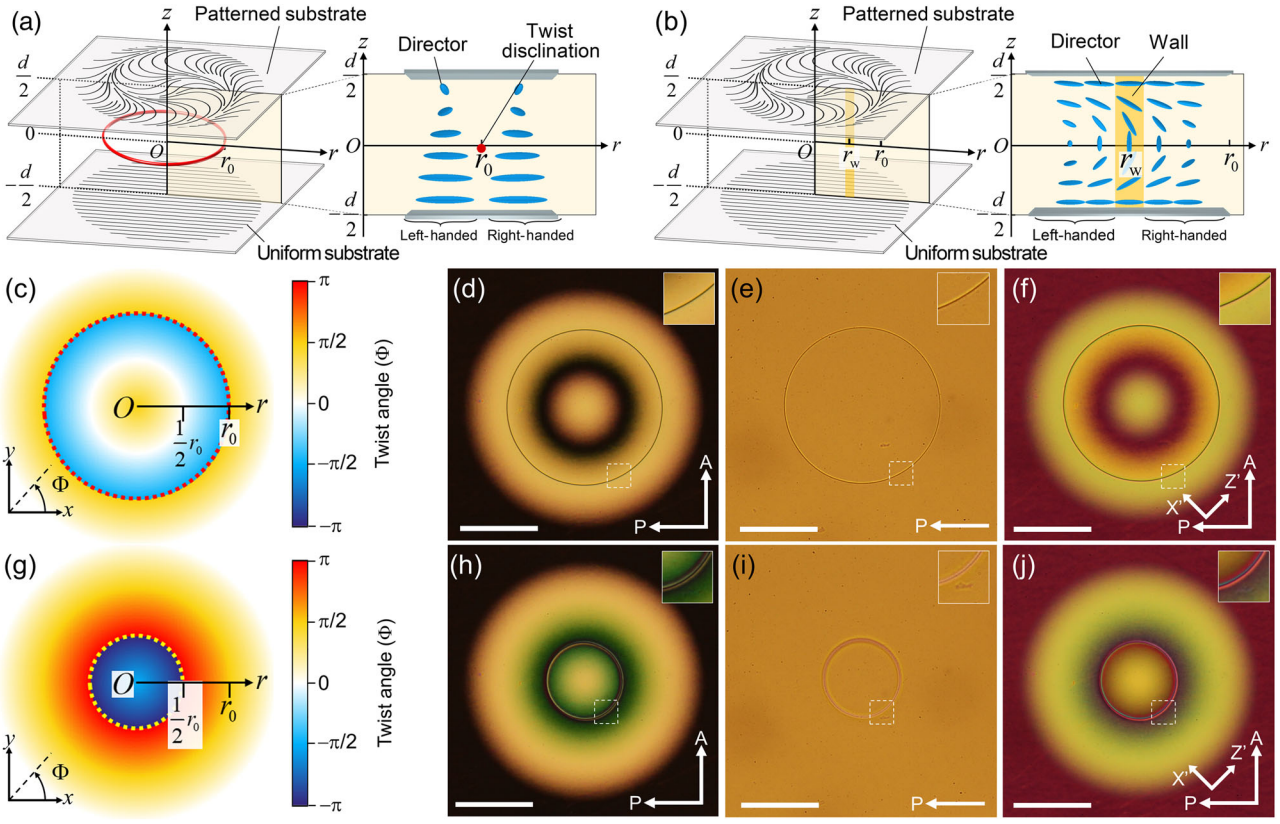

FIG. 2. Schematic of a LC cell with a (a) disclination loop and (b) wall loop. (c) Twist angle distribution between the substrates when a disclination is present. Microscope images of the disclination loop (d) between crossed polarizers, (e) without a polarizer, and (f) with a 530 nm retardation plate, where X' and Z' are the fast and slow axes. (g) Twist angle distribution between the substrates when a wall is present. Microscope images after wall generation (h) between crossed polarizers, (i) without an analyzer, and (j) with a retardation plate. Scale bars, 100 μm.

To satisfy the boundary conditions set by orientation patterning, we modify the Turner distribution and use the following, $\mathbf{n}_w(r,z)$, for a wall positioned at $r = r_w$:

$$n_{w,x} = \cos\left\{\pi\left[1+\left(-\frac{r}{r_0}+\frac{1}{2}\right)\tanh\left[m\left(r-r_w\right)\right]\right]\left(\frac{z}{d}+\frac{1}{2}\right)\right\},$$
$$n_{w,y} = \sin\left\{\pi\left[1+\left(-\frac{r}{r_0}+\frac{1}{2}\right)\tanh\left[m\left(r-r_w\right)\right]\right]\left(\frac{z}{d}+\frac{1}{2}\right)\right\}\tanh\left[m\left(r-r_w\right)\right],$$
$$n_{w,z} = \sin\left\{\pi\left[1+\left(-\frac{r}{r_0}+\frac{1}{2}\right)\tanh\left[m\left(r-r_w\right)\right]\right]\left(\frac{z}{d}+\frac{1}{2}\right)\right\}\mathrm{sech}\left[m\left(r-r_w\right)\right]. \quad (2)$$

The director changes its twist direction at $r = r_w$ as well as orienting perpendicular to the substrates, with a wall thickness defined by the parameter m (Sec. III of the SM [24]). Here we use the following for m, which minimizes the free energy for a parallel planar boundary condition [16]:

$$m = \frac{\pi}{d}\sqrt{\frac{K_{11}+K_{33}-2K_{22}}{3K_{22}+K_{33}}}. \quad (3)$$

In Sec. IV of the SM [24], we evaluate the topological charge of the modeled wall in a single r-z plane using Eq. (2) and show that it is indeed different from the disclination.

We numerically calculate the Oseen-Frank free energy of LCs, F, using $\mathbf{n}_w$ (Sec. V of the SM [24]) [1]. Figure 3(a) plots F as a function of r_w, where $d = 7.95$ μm, and $r_0 = 107.2$ μm as in the experiment, and $K_{11} = 4.85$ pN, $K_{22} = 3.1$ pN, $K_{22} = 3.1$ pN, $K_{33} = 6.1$ pN for 5CB [26]. F has a local minimum at $r_w = 48.7$ μm, which agrees with the experimental equilibrium radius at 49 μm. Note that the proposed mechanism yields an equilibrium radius that is always smaller than $r_0/2$, where, intuitively, the wall is likely to appear. In fact, Video 1 in the SM [24] shows a two-step transition for wall generation and stabilization, where the wall first appears at $r_0/2$ and then shrinks to the equilibrium position.

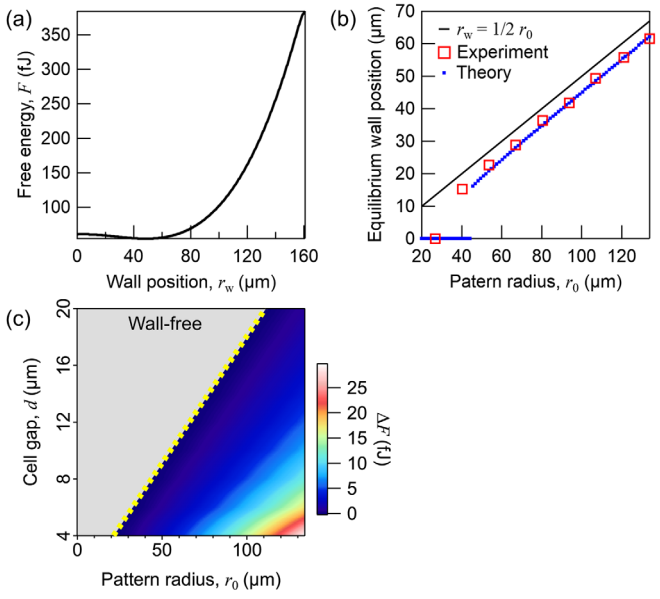

FIG. 3. (a) F vs r_w for a cell with $d = 7.85$ μm and $r_0 = 107.2$ μm. (b) Experimental and theoretical equilibrium wall positions vs r_0. The solid line indicates the ideal position of the wall with no shrinkage. (c) Stability of the director configuration with the wall loop relative to the wall-free state for different cell parameters. The dashed line indicates the crossover between the two configurations.

The validity of the model was investigated further by varying r_0 from 26.8 to 134 μm. Figure 3(b) compares the experimentally measured and theoretically predicted wall radii (the POM images shown in Sec. VI of the SM [24]). For $r_0 > 50$ μm, the experiment agrees well with theory, with the deviation between the two falling within 3%. For $r_0 = 40.2$ μm, the wall had an equilibrium radius of 15.2 μm, whereas theory predicted an equilibrium at $r = 0$, i.e., the director configuration without the wall to have lower energy. While this discrepancy is believed to be a result of $\mathbf{n}_w$ not fulfilling the Euler-Lagrange equations, we note that the energy difference between director configurations with and without the wall approaches 0 at the crossover of the stable state, which makes both configurations equally stable and thus prone to small fluctuations. Overall, the model reproduces the phenomenon more than satisfactorily, validating the stabilization mechanism.

We also investigate the effect of varying r_0 and d on the wall stability. Figure 3(c) shows stabilities of the director configuration with the wall relative to those without, where the dashed line represents the crossover condition of the stable configuration. Clearly, increasing stability is predicted for larger r_0 and smaller d, which can be attributed to the fact that the wall has to move over a greater area for larger r_0, and, the director twist rate, and hence the elastic energy penalty upon wall shrinkage, increases for smaller d. The results also allow us to infer that a steep change in twist angle near the wall stabilizes it since the energy rises quickly even for small shrinkage.

Finally, we extend our strategy to stabilize an arbitrarily shaped wall loop. Figure 4 shows disclination and wall loops stabilized in the shape of our school logo. The wall appears approximately where the substrates have parallel orientation, and its stability increases with a steeper

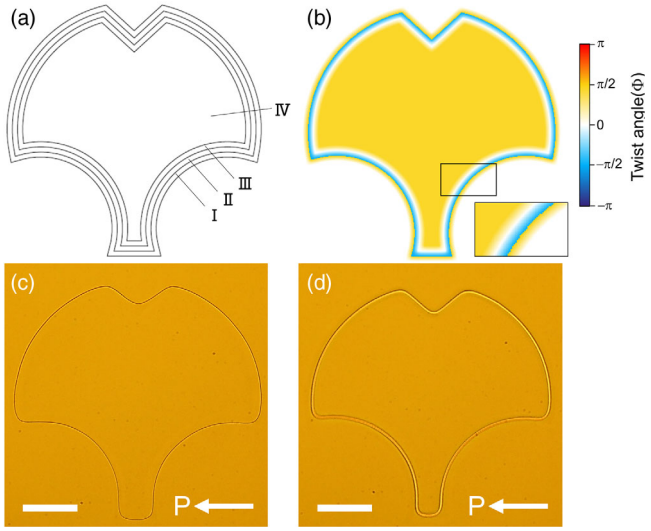

FIG. 4. (a) Osaka University logo divided into four areas. (b) Twist angle distribution to generate the wall loop. (c) Optical microscope image of disclination loop and (d) wall loop. Scale bars, 100 μm.

change in twist angle. Following this principle, we create four regions in the shape of the logo and obtain the easy axis distribution in each domain as numerical solutions to Laplace's equation. For the domains labeled I, II, and III in the figure, the outer and inner boundary conditions are set to $(0, -\pi/2)$, $(\pi/2, 0)$, and $(0, 4\pi/9)$. The sample first shows a disclination loop approximately at the boundary of domains I and II. Upon applying and removing an electric field, the disclination annihilates and a wall loop appears approximately at the boundary of domains II and III [Figs. 4(c) and 4(d); see also Sec. VII of the SM [24]]. This demonstrates the versatility of our approach, allowing meaningful symbols to be represented by stable walls.

In conclusion, we demonstrated a topology-mediated pathway for the generation of high-energy, nonsingular wall loops in a nematic LC. This Letter is distinct from other works in that a pure nematic LC with no inclusions was used in a planar cell structure, and the generated loop, which can be designed arbitrarily, is stable without a sustaining electric field. Other than motivating the search for designs to stabilize even higher energy defects, our Letter opens the door to detailed investigations of defect structure and dynamics [27], as well as their interaction with various dopants. Surface patterning allows positioning of the defect, which is usually not possible with colloid-induced defects, and thus is advantageous for potential applications of defects. Considering the fact that steep changes in the director affect not only the elastic energy of the system but also the dielectric and rheological properties, we anticipate the emergence of novel phenomena and applications through the investigation of defect-matter interactions in a controlled environment.

This work was supported by JST PRESTO (Grant No. JPMJPR151D) and JSPS KAKENHI (Grants No. 17H02766 and No. 19H02581). The authors thank the DIC Corporation for providing the photoalignment material and the JSR Corporation for providing the planar alignment material.

*Corresponding author.
yoshida@eei.eng.osaka-u.ac.jp

[1] P. G. de Gennes and J. Prost, *Physics of Liquid Crystals* (Oxford University Press, New York, 1993). 2nd ed.
[2] K. Mauice and O. D. Lavrentovich, *Soft Matter Physics: An Introduction* (Springer-Verlag, New York, 2003).
[3] B. Senyuk, Q. Liu, S. He, R. D. Kamien, R. B. Kusner, T. C. Lubensky, and I. I. Smalyukh, Nature (London) **493**, 200 (2013).
[4] S. Čopar and S. Žumer, Phys. Rev. Lett. **106**, 177801 (2011).
[5] M. Zapotocky, L. Ramos, P. Poulin, T. C. Lubensky, and D. A. Weitz, Science **283**, 209 (1999).
[6] H. Yoshida, K. Asakura, J. Fukuda, and M. Ozaki, Nat. Commun. **6**, 7180 (2015).
[7] B. Senyuk, J. S. Evans, P. J. Ackerman, T. Lee, P. Manna, L. Vigderman, E. R. Zubarev, J. van de Lagemaat, and I. I. Smalyukh, Nano Lett. **12**, 955 (2012).
[8] J. B. Fleury, D. Pires, and Y. Galerne, Phys. Rev. Lett. **103**, 267801 (2009).
[9] X. Wang, D. S. Miller, E. Bukusoglu, J. J. de Pablo, and N. L. Abbott, Nat. Mater. **15**, 106 (2016).
[10] X. Wang, Y. K. Kim, E. Bukusoglu, B. Zhang, D. S. Miller, and N. L. Abbott, Phys. Rev. Lett. **116**, 147801 (2016).
[11] T. Ohzono, K. Katoh, and J. Fukuda, Sci. Rep. **6**, 36477 (2016).
[12] K. Kawaguchi, R. Kageyama, and M. Sano, Nature (London) **545**, 327 (2017).
[13] J. Nehring, Phys. Rev. A **7**, 1737 (1973).
[14] R. B. Meyer, Philos. Mag. **27**, 405 (1973).
[15] R. Turner, Philos. Mag. **30**, 13 (1974).
[16] R. Turner, Phys. Lett. **49A**, 423 (1974).
[17] R. Turner, Philos. Mag. **31**, 719 (1975).
[18] A. de Lózar, W. Schöpf, I. Rehberg, D. Svenšek, and L. Kramer, Phys. Rev. E **72**, 051713 (2005).
[19] U. Tkalec, M. Ravnik, S. Copar, S. Zumer, and I. Musevic, Science **333**, 62 (2011).
[20] M. Cavallaro, M. A. Gharbi, D. A. Beller, S. Čopar, Z. Shi, T. Baumgart, and K. J. Stebe, Proc. Natl. Acad. Sci. U.S.A. **110**, 18804 (2013).
[21] M. Wang, Y. Li, and H. Yokoyama, Nat. Commun. **8**, 388 (2017).
[22] K. Sunami, K. Imamura, T. Ouchi, H. Yoshida, and M. Ozaki, Phys. Rev. E **97**, 020701(R) (2018).
[23] D. W. Berreman and W. R. Heffner, Appl. Phys. Lett. **37**, 109 (1980).
[24] See Supplemental Material at http://link.aps.org/supplemental/10.1103/PhysRevLett.123.097801 for description of the director models (Secs. I–III); comparison of the topological charges of the disclination and wall

(Sec. IV); calculation methods (Sec. V); and additional experimental data for Figs. 3 and 4 (Secs. VI–VII).

[25] C. Jones, in *Handbook of Liquid Crystals*, edited by J. W. Goodby, P. J. Collings, T. Kato, C. Tschierske, H. Gleeson, P. Raynes, and V. Vill (Wiley-VCH, Weinheim, 2014), 2nd ed., Vol. 8, Chap. 4.

[26] D. A. Dunmer, in *Physical Properties of Liquid Crystals: Nematics*, edited by D. A. Dunmer, A. Fukuda, and G. R. Luckhurst (INSPEC, London, 2001), Chap. 5.2.

[27] M. Ambrožič, S. Kralj, and E. G. Virga, Phys. Rev. E **75**, 031708 (2007).